Structure and Mechanics of Membrane Proteins

Andreas Engel[1] and Hermann E. Gaub[2]

[1]Maurice E. Müller Institute for Structural Biology, Biozentrum, University of Basel, 4056 Basel, Switzerland; email: andreas.engel@unibas.ch

[2]Center for Nanoscience and Physics Department, University Munich, 80799 Munich, Germany; email: gaub@lmu.de

Annu. Rev. Biochem. 2008. 77:127–48

The *Annual Review of Biochemistry* is online at biochem.annualreviews.org

This article's doi: 10.1146/annurev.biochem.77.062706.154450

0066-4154/08/0707-0127$20.00

Key Words

atomic force microscope, bacteriorhodopsin, folding potential, ligand binding, scanning electrochemical microscope, single-molecule force spectroscopy

Abstract

Evolution has tuned membrane proteins to exist in a lipid bilayer, provide for cell-cell communication, transport solutes, and convert energies. These proteins exhibit a hydrophobic belt that interacts with the lipid bilayer. Detergents are therefore used to extract membrane proteins and keep them in solution for purification and subsequent analyses. However, most membrane proteins are unstable when solubilized and hence often not accessible to NMR or X-ray crystallography. The atomic force microscope (AFM) is a powerful tool for imaging and manipulating membrane proteins in their native state. Superb images of native membranes have been recorded, and a quantitative interpretation of the data acquired using the AFM tip has become possible. In addition, multifunctional probes to simultaneously acquire information on the topography and electrical properties of membrane proteins have been produced. This progress is discussed here and fosters expectations for future developments and applications of AFM and single-molecule force spectroscopy.

Contents

INTRODUCTION

Biological membranes enclose and compartmentalize cells of all organisms, acting as effective insulators and selective filters between the cytoplasm and the outside medium. Composed of a phospholipid double layer, each membrane houses particular proteins or protein complexes that provide specific communication channels between the compartments or the cell and its environment. Lipids and membrane proteins form domains, which can vary and adapt to the functional state of the cell (1, 2). Membrane proteins, often arranged in lipid-protein domains, are involved in basic cellular activities, such as solute and ion transport, energy transduction in respiratory and photosynthetic systems, or sensory stimuli transduction and information processing; hence, they are important drug targets. Although ~30% of all genes are known to encode membrane proteins, our understanding for this important class of proteins lags behind because of their highly hydrophobic nature, their intricate subunit structure, and their resistance to assemble into three-dimensional crystals suitable for X-ray analysis. Both their individual polypeptide composition as well as their specific assembly into larger protein complexes, i.e., their quaternary structure in the membrane, are fundamental aspects in the molecular description of their functionality. As result of their insolubility in aqueous media, the analysis of membrane proteins is notoriously difficult. Detergent treatment is required for solubilization and purification, the latter being a prerequisite for most structural studies. Yet detergent-solubilized membrane proteins are often unstable and tend to aggregate, and they may or may not be in their native conformation. Methods that allow membrane proteins to be assessed in the native membrane or when reconstituted in a lipid bilayer are thus of interest.

Atomic force microscopes (AFMs) are tools to address the surface structure and mechanics of single-membrane proteins in their native environment, i.e., embedded in the lipid bilayer and immersed in a physiological salt solution (3). Not only are the surface structure, the supramolecular arrangement, and the lateral organization of the proteins revealed, but moreover individual proteins may be addressed and investigated in greater detail. They may be contacted by the AFM tip and subsequently extracted from the membrane (4). The forces that keep the protein in the membrane as well as those that resist unfolding of the protein may thus be studied with unparalleled resolution and sensitivity (5). The unfolding barriers may be localized in the sequence with an accuracy of a few amino acids, and the folding energy landscape can be analyzed both in magnitude but also in the dynamics of the response. The binding of individual ligands may be visualized, and the alterations in the mechanics of the proteins may be detected and localized, again with the precision of a few amino acids. Not only unfolding processes may be followed, but also controlled refolding of the proteins

into the membrane can be achieved. The unfolded polypeptide chain is gradually allowed to sink back into the membrane while the force at which it is pulled into its native environment is recorded. Nonequilibrium aspects of such folding/unfolding cycles reveal details on kinetics and dynamics of the underlying processes.

INSTRUMENTATION

Invented three decades ago (6), scanning probe microscopes have been applied in many areas, and their capabilities have constantly been refined and optimized for specific applications. The principle of the AFM is simple: A sharp tip mounted at the end of a flexible cantilever is raster scanned over a sample surface, and the cantilever deflection caused by the probe-sample interaction is measured via an optical system. This signal drives a servosystem that moves the sample vertically to keep the cantilever deflection at a constant value. The surface topography is then reconstructed from the vertical movement of the scanner. In this mode, the probing tip always presses on the surface with a constant force during scanning (7). Alternatively, the AFM tip is oscillated rapidly in the vertical direction while scanning the sample. When the tip approaches the sample surface, a reduction in the oscillation amplitude is measured and used to control the servosystem. The tip oscillation reduces frictional forces, thereby minimizing damage and displacement of the sample (8). Therefore, the oscillating mode is frequently used to image the surface topography of weakly immobilized biomolecules, e.g., single proteins and fibrillar structures. An even more sensitive variant of the oscillating mode is the dynamic mode AFM, whereby frequency shifts of the oscillating cantilever resulting from tip-sample interactions are measured and used as a feedback signal for the servosystem (9). The major advantage of all these imaging modes is that they can be executed in fluids, thus allowing biological macromolecules to be observed at work.

Progress in instrumentation concerns AFMs that provide high scan speed (10–11a), higher force sensitivity (9), and acquisition of multiple signals received simultaneously (12). Operation in fluids imposes limitations and brings about technical difficulties. First, cantilevers that exhibit a Q-factor of about 10^4 in a vacuum, and some 10^2 in air, have a Q-factor of <10 when operated in solution (13). Because the force sensitivity depends on the Q-factor, such a decrease is critical. Second, the resonance frequency of a cantilever drops by a factor of about five in liquid from its value in a vacuum. Hence, the scan speed must be correspondingly reduced for scanning in liquid. Third, conducting cantilever for measurements of a chemical reaction in solution need to be properly insulated, which requires complex microfabrication procedures. Nevertheless, several successful designs toward fast AFMs have been reported, and encouraging results have been published. Fast-scanning AFMs recording up to 1300 topographs per second may in future help capture the fast dynamics of membrane proteins (10–11a, 14). Moreover, progress in scanning electrochemical microscopy (SECM) suggests that electronic activation and direct observation of biological processes at the molecular level are feasible. These developments are closely linked to improved cantilever fabrication; small cantilevers are key to fast scanning, whereas insulated cantilevers with metal tips are needed for high-resolution SECM.

HIGH-RESOLUTION IMAGING OF MEMBRANE SURFACES

Several factors affect the spatial resolution achieved by AFM. First, membranes need to be immobilized on a flat supporting surface because a soft membrane adsorbed onto a support will adapt to the modulation of the supporting surface. Muscovite mica is the most frequently used support in AFM. Cleaving the layered mica crystal provides highly reproducible atomically flat surfaces that allow

adsorption of membranes to be tuned by ionic strength and pH (15, 16). Second, high-resolution AFM imaging of fragile biological surfaces requires precise control of the tip-sample interactions and the parameters of the servo system that guide the AFM stylus over the object. In particular, the electrostatic interactions between AFM stylus and biological sample must be adjusted to distribute the excess scanning force applied over an area that is perhaps 10 times larger than that of the tip apex itself (17). Third, to identify a suitable tip requires patience and experience (16). Last but not least, the instrument must be stable and shielded from vibrations and noise, all critical surfaces must be clean, and the electronic feedback parameters must be properly adjusted (16).

Imaging Native or Reconstituted Two-Dimensional Membrane Protein Crystals

Purple membranes of *Halobacterium halobium* are ideal objects to explore the capability of an AFM and to optimize the imaging conditions. These highly specialized membranes are a native two-dimensional trigonal lattice assembled from lipids and bacteriorhodopsin, the archaeal proton pump. An early example (18) is shown in **Figure 1**, which summarizes the capability of an AFM to depict and manipulate single-polypeptide loops that connect the seven transmembrane α-helical segments, constituting the protein. Under optimized conditions, the AFM allows a lateral resolution of ≈0.5 nm and a vertical resolution of ≈0.1 nm to be achieved, as demonstrated in several instances (19). The exceptionally high signal-to-noise ratio of the AFM allows structural details of single-membrane proteins to be observed and the flexibility of protrusions, comprising a small number of amino acid residues, to be assessed quantitatively (20).

Other examples concern halorhodopsin, a protein that is related to bacteriorhodopsin (21), and many reconstituted mostly regularly packed membrane proteins. High-resolution topographies have been acquired on porin OmpF (22, 23), staphylococcal α-hemolysin (24), aquaporins (25–27), rotors from various F_0 ATP synthases (28–30), and bacterial light-harvesting complexes (31, 32). Because most of the high-resolution topographs were initially achieved on membrane proteins that were crystallized in two dimensions, it was thought that a crystalline assembly would be a prerequisite for observing membrane proteins at subnanometer resolution by AFM. However, it was demonstrated that a comparable spatial resolution can be achieved on noncrystalline assemblies of membrane proteins (30, 33), suggesting that native membranes might be imaged at high resolution as well.

Imaging Native Membranes

In almost all methods available today to analyze membrane proteins at high resolution, the protein needs to be solubilized, purified, and further processed to be amenable to analysis. In this respect, the AFM is a unique exception, as it allows the surfaces of native membranes to be scanned and the protein surfaces to be resolved down to the subnanometer level without dissassembling the biological membrane. Therefore, once this approach was developed, the AFM quickly provided new insights into the native organization of membrane proteins and their complexes

Rhodopsin. The first breakthrough in imaging native membranes was achieved when disk membranes prepared from mouse retina and deposited on mica could be imaged by an AFM at sufficient resolution to identify the native packing arrangement of rhodopsin (**Figure 2*a***) (34). Rhopdopsins were found to arrange in rows of dimers, thereby providing a platform for interaction with arrestin as well as with the G protein heterotrimer (35). As this finding is in stark contrast to previous measurements on the function of G protein–coupled receptors (GPCRs), these observations have a significant impact. The

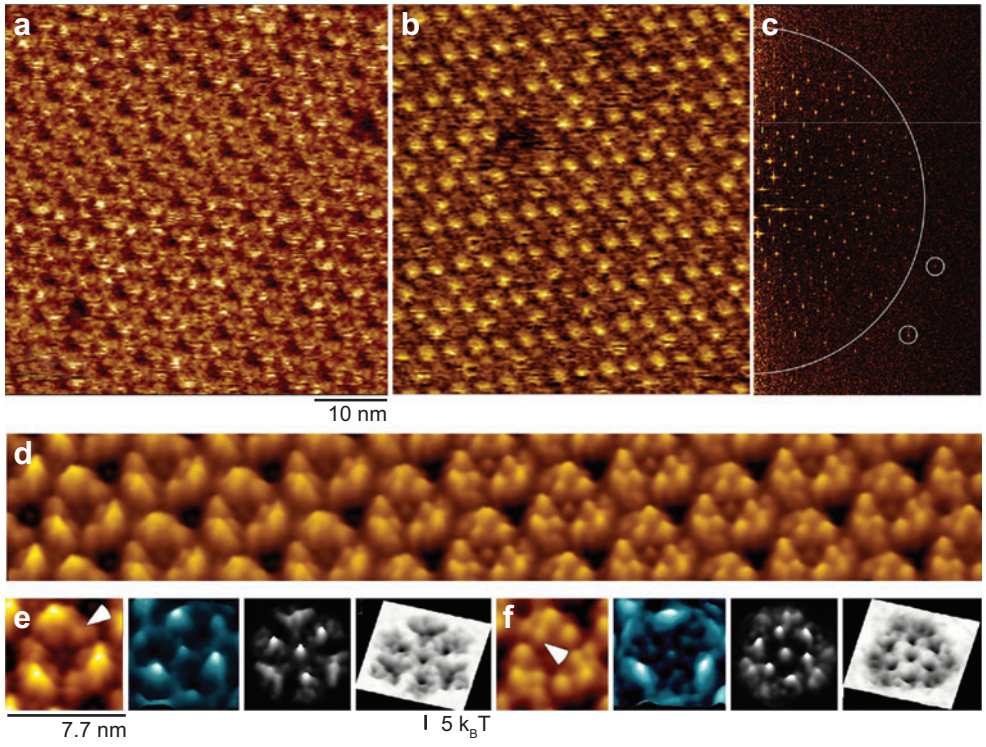

Figure 1

AFM topographs of purple membrane adsorbed to mica (19). (*a*) High-resolution topograph of the cytoplasmic surface of the trigonal lattice revealing bacteriorhodopsin trimers. During the scan, the force applied to the stylus was varied from ≈50 pN (*top*) to ≈100 pN (*upper half*), to ≈50 pN (*center*), and to ≈100 pN (*lower half*). The conformational change is significant, yet fully reversible (18). (*b*) The extracellular purple membrane surface is more stable than the cytoplasmic one because the prominent protrusion is formed by a compact β-hairpin [see Protein Data Bank (pdb) entries 2AT9 and 1f50]. Bacteriorhodopsin trimers are prominent, as is the defect in the lattice, where one trimer is missing. (*c*) The diffraction pattern of panel *b* indicates a lateral resolution of better than 0.5 nm (spots marked by circles outside the 0.5 nm half circle). (*d*) To demonstrate the force-induced conformational change of the cytoplasmic bacteriorhodopsin surface, respective averages from low (*left*) to high force (*right*) have been morphed. (*e*) Analysis of the low-force state of the cytosolic bacteriorhodopsin surface. The following are shown from left to right: correlation average, standard deviation (SD) map, probability map of loop locations, and related surface energy potential. The SD and probability maps show that the E-F loop, which is the prominent protrusion at the periphery of the trimer, is rather flexible. Therefore, a large SD is observed at the site of the E-F loop, and a wide distribution of its possible positions is seen in the probability map. This translates into a shallow potential trough in the surface energy map. In contrast, loop A-B (*arrowhead*) is well localized, leading to a small signal in the SD map and a sharp peak in the probability map. (*f*) Analysis of the high-force state of the cytoplasmic bacteriorhodopsin surface. The following are shown from left to right: correlation average, standard deviation (SD) map, probability map of loop locations, and related surface energy potential. The location of the E-F loop still reveals a high SD, yet a new stable feature is now unveiled in this region, the C-D loop (*arrowhead*). A central well-localized signal in both conformational states is related to the presence of a lipid molecule at the threefold axis. The width of all maps in panels *e* and *f* is 7.7 nm, and the vertical bar indicates 5 k_BT (20). All topographs were recorded at room temperature in buffer solution.

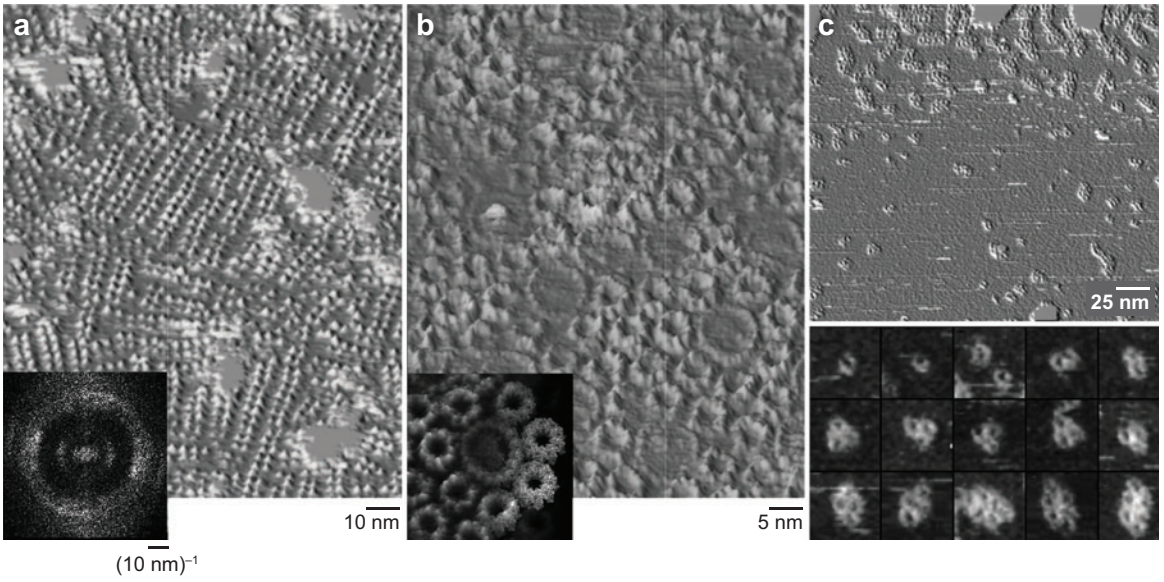

Figure 2

AFM topographs of native membrane adsorbed to mica. (*a*) Disc membrane from mouse retina (34, 35). Rows of rhodopsin dimers are distinct, but this observation is in stark contrast to early fluorescence recovery after photobleaching experiments, which suggested the existence of a major rhodopsin monomer fraction. Yet, many recent observations support the hypothesis that G protein–coupled receptors act as dimers or higher oligomers (40, 41). The inset shows the power spectrum from which the relevant distances of the paracrystals were determined (34). (*b*) Native photosynthetic membranes of *Rhodospirillum photometricum* (45, 51). Large light-harvesting complex 1 (LH1) rings and small LH2 rings pack tightly. On the basis of such topographs, an atomic model of the photosynthetic machinery was established (inset) (104). (*c*) Outer mitochondrial membranes reveal voltage-dependent anion channels (VDACs) in different oligomeric states (53). The use of the frequency-modulated dynamic-imaging mode (9) allowed topographs of single VDACs to be recorded.

issue whether GPCRs are active as a monomer or as a higher oligomer is, however, not resolved. Cross-linking experiments performed on native disk membranes (36) did not contradict the notion of rhodopsin dimers, whereas cysteine scans combined with cross-linking assays on the dopamine D2 receptor provide compelling support for the model derived from the AFM topographs (37). Functional assays on rhodopsin solubilized by maltoside detergents exhibiting different alkyl chains revealed a 10-fold increase in G protein activation when rhodopsin was solubilized as a higher oligomer (38). It emerges from many observations that not only rhodopsin works as a dimer (39) but that GPCRs in general function as homo- or even heterodimers (40, 41), a notion that is currently challenged by different approaches (42, 43).

Photosynthetic membranes. Topographs of native membranes acquired by AFM have provided new information on the architecture of the photosynthetic apparatus in different photosynthetic bacteria (reviewed in Reference 32). Images of sufficient resolution to see individual subunits have been recorded on membranes from *Rhodopseudomonas viridis* (44), *Rhodospirillum photometricum* (45), *Rhodobacter sphaeroides* (46), *Rhodobacter blasticus* (47), *Phaeospirillum molischianum* (48), and *Rhodopseudomonas palustris* (49). Using the atomic structures of individual components, atomic models of the light-harvesting and

light-driven proton-pumping systems have been established (**Figure 2*b***) (50), which allow energy transfer mechanisms to be scrutinized. A fascinating observation concerns the structural changes of the photosynthetic apparatus during chromatic adaptation of *R. photometricum* to high-light and low-light growth conditions. AFM images revealed that under normal light levels core complexes gather in membrane domains with ~3.5 LH2 rings per core without being in a fixed regular architecture. Under low-light conditions, however, additional LH2 complexes assemble in paracrystalline antenna domains (51).

Mitochondrial outer membranes. The outer mitochondrial membrane houses specific proteins, which facilitate metabolic coupling and signaling between the cytosol and mitochondria. This membrane must be tight because stress-induced release of cytochrome *c* leads to apoptosis. A major part of the molecular traffic is mediated by the voltage-dependent anion channel (VDAC), a general diffusion pore exhibiting a diameter of 2–3 nm. These porins have a molecular mass of around 30 kDa per functional channel and have been found in all eukaryotic organisms. For membrane potentials > |20 mV|, VDACs are in a state that has a reduced conductance. Electron microscopy has shown that these pores form lattices whose unit cells comprised 6 VDACs when native mitochondrial outer membranes were treated by phospholipase A_2 (52). However, only recently has it been possible to reveal these channels directly in the native outer membranes of mitochondria from potato (53) and from yeast (54). In some membrane domains, VDACs were found to be packed at high density like bacterial outer membrane porins (54), whereas in other domains, VDACs were loosely packed, exhibiting single pores and oligomeric clusters comprising two, three, four, and six channels (**Figure 2*c***) (53). Of interest is the observation that the frequency-modulated AFM mode yielded the best images of VDACs, in particular of single pores that were difficult to visualize in contact mode, probably as result of lateral friction forces (53).

SIMULTANEOUS ACQUISITION OF SURFACE TOPOGRAPHY AND CURRENTS

The dream of structural physiologists and biophysicists is the simultaneous observation of a current and the conformational changes of the related biomolecular machinery at the single-molecule level. Voltage- or low-pH-induced conformational changes of the extracellular loops were speculated to lead to channel closure for the bacterial outer membrane porin OmpF (22). Later, the pH-driven closure of maltoporin was demonstrated by black-lipid membrane experiments (55), and the structure of an open and a closed conformation of porin OmpG showed the involvement of extracellular loops (56). However, concomitant observation of current and conformational changes have not been possible. Only recently, the fabrication of cantilevers with a conductive tip and insulated lead, which are stable in salt solutions and exhibit suitable mechanical properties, was established (57). Initial experiments demonstrated that the topography of a biological sample and faradaic currents can be acquired simultaneously with a lateral resolution of 3–8 nm using such cantilevers (**Figure 3**) (12). They are operated in an electrochemical setup employing a bipotentiostat to monitor redox processes (58). A critical element is the support, which should release or accept electrons from a soluble redox couple, should be stable over the time required to conduct the redox experiment, should be inert to preserve the structure and function of the biomolecule, and should be atomically flat for high-resolution imaging. Only a few materials have been found suitable, and among them template-stripped Au and Pt surfaces are probably the best (P. Frederix & P. Bosshart, personal communication). Protein-lipid membranes covering

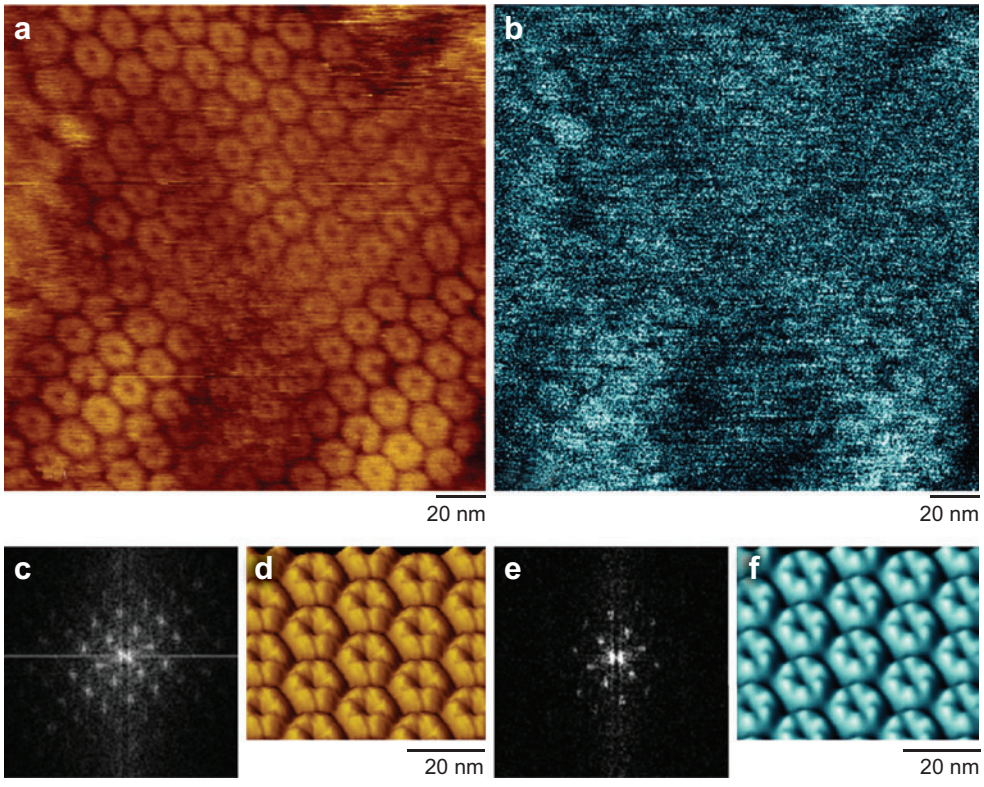

Figure 3

Simultaneous recording of surface topography and faradaic currents using a multifunctional cantilever (12). (*a*) The hexagonally packed intermediate (HPI) layer was recorded with an insulated Pt tip clamped at −750 mV in buffer solution (225 mM KCl, 20 mM Tris-HCl, pH 7.3). The bias voltage was important not only to induce a current, but also to obtain high-resolution images. (*b*) Concomitant current recordings produced a current density map, which reveals the HPI doughnuts, but the data recorded is noisy. The current was reduced by <0.25 pA when the tip was lowered into the trenches between protruding HPI hexamers. This reduction is scaled to a height difference of <1.8 nm measured on the topograph shown in (*a*) and corresponds to the current-distance calibration during an approach to the HPI layer on the highly oriented pyrolytic graphite (HOPG) support. (*c*) Diffraction pattern of the topography in panel *a* shows reflections to about $(3.3\ \text{nm})^{-1}$. (*d*) At this resolution, the correlation average of panel *a* shows the typical features of the HPI hexamer. The vertical scale given by color shades is 1.8 nm. (*e*) Owing to the noise, diffraction spots are visible in the power spectrum of the current map in panel *b* only to a resolution of $(7.8\ \text{nm})^{-1}$. (*f*) Because the current was simultaneously recorded with the topography, the processing parameters of the latter were applied to calculate the correlation average of the current density map. The vertical scale given by color shades is 0.25 pA.

a hole (59) or a nanowell (60) appear to be an interesting alternative to establish an electrochemical gradient for the assessment of membrane-bound molecular redox machines, although high-resolution imaging on a lipid-embedded membrane protein array will be difficult.

UNFOLDING OF INDIVIDUAL MEMBRANE PROTEINS

Advances in single-molecule force spectroscopy of soluble proteins and cells tethered between a support and a cantilever (61) have stimulated experiments on bacterial surface layers (62, 63) and on bacteriorhodopsin (4).

As illustrated in **Figure 4**, these experiments not only provided information on the unfolding forces, but also revealed the structural changes related to the extraction of a single-membrane protein using the AFM tip as nanotweezer. Two different strategies for the attachment of individual proteins to the AFM tip were reported in single-molecule force spectroscopy experiments: physisorption (64) or covalent bonding via reactive groups (4). Physisorption between the tip and protein was found to be initiated when the repulsive tip-sample interaction is overcome by increased contact force (65). Although details of the underlying mechanisms are unclear, the breakdown of the hydration shells of both the protein and the tip is generally believed to be the dominant mechanism that triggers adhesion. The finding that physisorbed molecules may withstand pulling forces of several hundred pN before they detach indicates that multiple local interactions based on van der Waals forces, charge interactions, and hydrogen bonds stabilize this contact (66, 67). When the nN force regime needs to be probed, the proteins must be covalently attached, preferably via known natural or site-specifically introduced reactive amino acids, e.g., cysteins (68, 69). The covalent attachment not only allows an extended force range to be explored with the consequence of a prolonged time window for the experiments, but it also enables precise and absolute length measurements during the unfolding process (4).

For the investigation of membrane proteins, both strategies have proven to be useful (4, 70). While imaging the membrane proteins at high resolution, individual proteins were selected. Scanning was halted, and the selected protein was then contacted by increasing the force beyond the adhesion threshold, which was found to differ from system to system but lies typically in the range of 100–200 pN. Upon retracting the tip, a force distance trace was recorded as a protocol for the unfolding and extraction process. A subsequent imaging of the sample allowed experiments where a single-membrane protein was extracted to be identified, and the corresponding force distance traces to be selected for further analysis (see **Figure 4**). With no specific functionalization, this analysis showed that proteins were picked up at random positions of the protein surface, typically at the loops. Therefore, a detailed analysis required traces to be selected, which showed the full length of the unfolded protein, identifying those measurements where the protein was picked up at the terminal end of the protein (4). The force distance traces were then sorted by their length and only those traces with the full length of the completely unfolded protein were further analyzed. These long traces have exclusively in common that the protein is attached to the tip at the C-terminal end. An alternative strategy to preselect the attachment site was chosen by introducing a cysteine in the cytoplasmic tail and allowing this group to bind to the gold-coated tip. Oesterhelt et al. (4) reported an increase in the percentage of full-length traces to 90%, however, at the price of a reduced image resolution and a drastically decreased lifetime of the tip. An additional very interesting issue arose in the discussion on how the load acting on the protein is distributed in the membrane. Whether those parts of the protein on the opposing side of the membrane locally interact with the supports or whether the membrane bending elasticity is high enough to distribute the force over a larger area were major concerns. Experiments on multiple membrane stacks unambiguously showed that the stiffness of the membrane is sufficient and that, under suitable conditions, the adhesion between the lower loops and the supports can be reduced below the force resolution limit (70). As a result, a multitude of membrane proteins was investigated by single-molecule force spectroscopy, and the force distance traces provided a richness of novel information that would not have been accessible otherwise (71–77).

Unfolding of filamentous proteins, such as titin (64) or recombinant tandem constructs

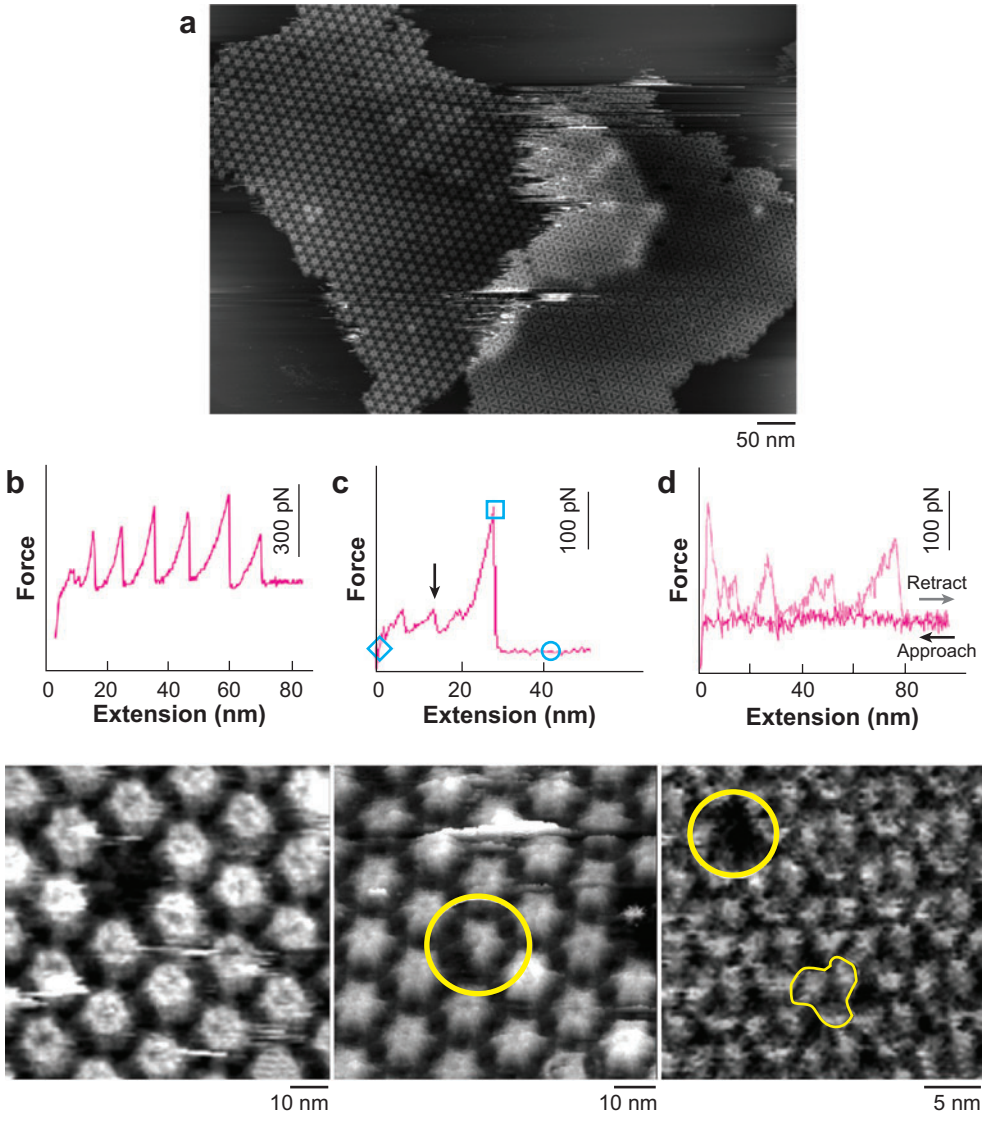

Figure 4

Unzipping individual proteins from a regular array and subsequent high-resolution imaging of the respective vacancy. (*a*) The overview of the surface (S-) layer from *Corynebacterium glutamicum* shows an ideal sample for imaging/single-molecule force experiments because both sides of the layer are accessible to the tip (63). (*b*) A distinct relation between the number of force peaks and the related damage is observed on the hexagonally packed intermediate (HPI) layer (62). Six single peaks and the vacancy corresponding to one hexamer indicate that each force peak corresponds to the removal of one HPI protein. Because one unit contains about 900 residues, only the peptide bridges, holding the HPI proteins together as hexamers, unfold. (*c*) Similar observations on the S-layer from *C. glutamicum* reveal more complex force peaks: dislodging two subunits required one small (*arrow*) and one fivefold larger force peak (63). (*d*) Unzipping a single bacteriorhodopsin molecule produces a series of force peaks that can unambiguously be related to the seven-transmembrane α-helical structure of bacteriorhodopsin (4).

of globular proteins (78, 79), consists of multiple events related to domains that sequentially denature upon forced unfolding in an order determined by the mechanical stability of the respective segments. For membrane proteins, their primary structure predetermines the sequence of the unfolding events (78, 80). Barriers may be overcome by thermal fluctuations without showing their characteristic signature in the individual unfolding traces. However, because only the next barrier in the sequence is loaded, the order at which they unfold cannot even partially be reversed. The assignment is thus less error prone, and as an additional consequence, the precision at which the barriers can be assigned is higher in membrane proteins than in the filamentous proteins.

Localizing Unfolding Barriers

In the course of protein unfolding, the force that the cantilever exerts on the protein is transmitted along the backbone into the membrane protein. The protein is stabilized in its conformation by the interplay between local forces, which in their complexity are represented by the potential energy landscape. When the protein is pulled upon, it is dragged in the 3N-dimensional energy landscape along a chosen direction and encounters a barrier, which needs to be overcome to continue the unfolding process. Two contributions act together in this process: the external force, which is transmitted through the backbone of the already unfolded part of the protein, and thermal fluctuations. Two strategies arise to overcome this barrier: force or patience. The latter increases the likelihood that thermal fluctuations will overcome the remaining barrier. If in addition an external force is applied, the barrier will be overcome at lower forces, and as a consequence, the force needed to overcome the barrier will depend on the rate at which the force is increased (81, 82). Because the AFM allows control of the position of the tip with angstrom precision, one strategy to determine the barrier location could be to measure the length of the already unfolded part of the membrane protein and calculate back to the position of the barrier in the primary structure (see **Figure 5*b***). However, two effects alter the apparent length of the unfolded protein under load: backbone elasticity and thermal fluctuations. For an analytical approach, a description of the statistical mechanics of the polymer in a thermal bath combined with a local enthalpic elasticity is needed as is discussed below.

An alternative approach for the localization of the potential barriers, which includes all these length scales, was opened recently by molecular dynamics calculations under an external force. The laboratories of Helmuth Grubmüller (83, 84) and of Klaus Schulten (85) have pioneered this field and resulted in full atomic representations of the proteins calculated in aqueous ambient solutions. Important details, such as the rupture of hydrogen bonding systems (86) or hierarchies of unbinding events (87), were shown and helped significantly to develop a better understanding of these molecular systems. Despite the obstacle that the available time window is still limited, the calculated and the measured force distance traces converge with increasing computational power and provide hope for a detailed picture of demanding systems, e.g., membrane protein complexes.

Ab initio Description of the Elasticity of the Polypeptide Backbone

At a given force, the elasticity of the covalent bonds in the amino acid backbone gives rise to an increase in its length. At the same time, thermal fluctuations kick the backbone, which on average pulls the cantilever closer to the membrane. Several models have been developed to quantify this entropic elasticity of unfolded proteins. The most commonly used approach is based on the worm-like chain model (88). Here the polymer is treated as an elastic rod with bending stiffness. Thermal fluctuations bend the rod and as a result decrease the end-to-end distance of the rod.

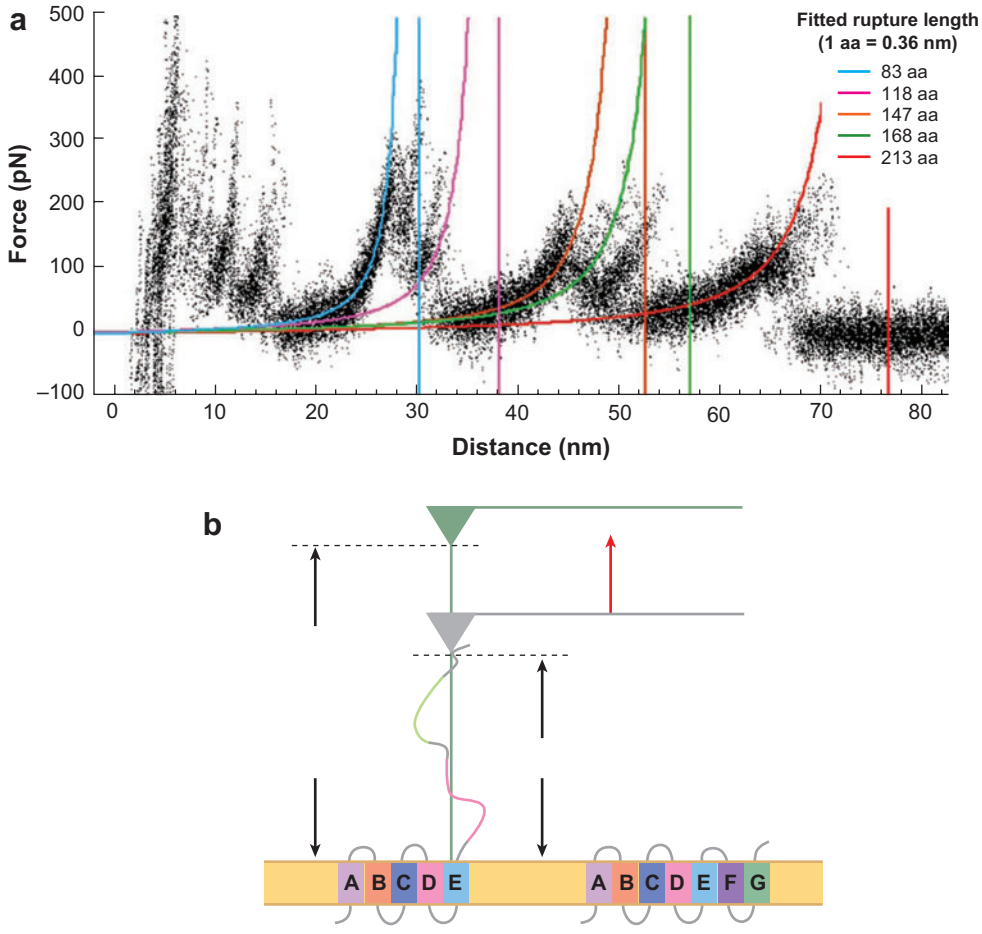

Figure 5

Analysis of the force distance traces of bacteriorhodopsin molecules. (*a*) Twenty-four curves were superimposed to highlight the common features of the individual traces. Solid lines represent the calculated force distance curves for the best contour length of the unfolded part of the protein, marking the different folding barriers. (*b*) Cartoon of the unfolding process. From the measured force distance traces the contour length of the unfolded part of the protein is calculated. With the known sequence, the position of the unfolding barrier can be localized in the structure (4, 81).

As a consequence, a force builds up when the ends are kept at a certain distance. With many such elements in series, the ensemble average then allows modeling of the force-distance relation of an unfolded protein. Alternatively, the entropy elasticity was treated in the freely jointed chain model (65). Here, the conformational freedom of jointed segments with random orientation was calculated as a function of the end-to-end distance. In the time-average, the entropic penalties for rare conformations increase the Gibbs free energy and give rise to a restoring force. For long polymers and moderate distortions from the thermal average, both models have been shown to be equivalent descriptions. A third, more realistic description was introduced by Kreuzer at al. (89), the freely rotating chain model. It allows the free rotation of segments of a fixed length with a certain angle. This model comes closest to reality but was solved analytically only recently (90).

All purely entropic models were shown to deviate from the measured extensions at higher forces. In some instances, the chemical nature of the polymeric backbone leaves marked fingerprints (91, 92). The backbone elasticity was in a first attempt modeled in a linear approximation with empirically derived segment elasticities. These "enthalpic" terms were added to the entropic description and provided a satisfactory agreement between theory and experiment but required empirical fit parameters. Some of them, like the extremely short persistence length in the combined worm-like chain (WLC) model, lacked stringent rationality. Netz and coworkers (93) therefore employed ab intitio quantum mechanical methods to calculate the elasticity of the most abundant biopolymer backbones, the polyamino acids, and the polynucleic acids and compared them with a simple polycarbon backbone. For this purpose, they computed with increasing levels of accuracy the energies of the different backbone segments for different lengths. From the length-dependent energies, they derived the force-dependent extensions and fitted the numerical results with second-order polynomials. Both contributions, the increase in bond length as well as changes in the bond angles, were found to contribute to the elasticities. The results are summarized in the graphs in **Figure 6**.

The combination of parameter-free ab initio elasticities with the freely rotating chain model, which (with the knowledge of the chemistry and the rotational degrees of freedom of the segments) is also parameter free, now provides for a parameter-free fit of the contour length of biopolymers (94). Particularly for the unfolding experiments described

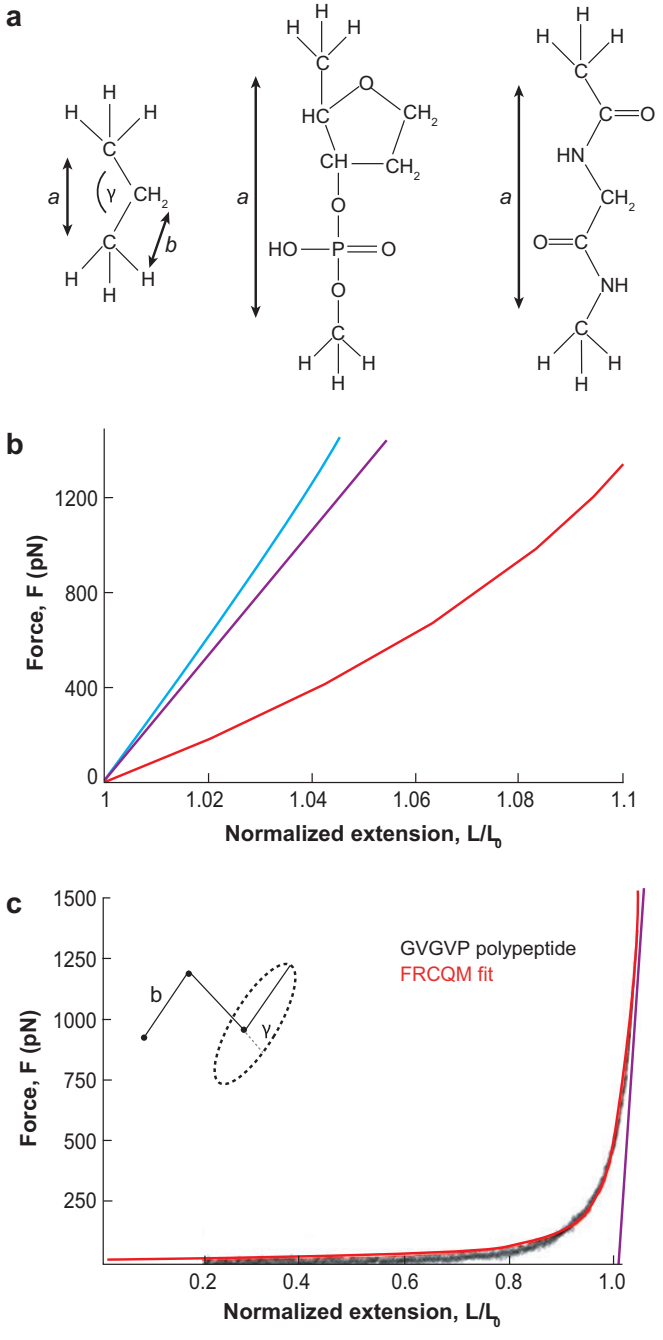

Figure 6

Parameter-free description of the elasticity of different biopolymers. (*a*) Schematics of the alkanes, polynucleic acids, and polyamino acids. (*b*) Ab initio quantum mechanics calculation of the force versus the extension relations of the three biopolymer monomers. Blue line, polyamino acids; purple line, alkanes; red line, polynucleic acids. (*c*) The segment elasticity of the protein backbone was combined with the freely rotating chain (FRC) model to account for the full range of the extensibility (*red line*). Plotted in comparison is a measured extension trace for a model peptide (105).

above, this approach allows the series of peaks in the force distance curves to be fitted and the contour lengths of the unfolded stretches of the membrane protein to be determined. With this procedure, Kessler & Gaub (95) were able to localize the unfolding barriers in bacteriorhodopsin with the precision of 3 amino acids (see **Figure 5*a***).

Further details on the nature of these barriers were obtained by experiments with a varied force loading rate. Müller et al. (96) analyzed the barrier heights and the spontaneous unfolding rates of the major barriers in bacteriorhodopsin. They also analyzed the temperature dependence of the unfolding peaks and derived a hierarchy of the thermal stabilities of the corresponding structural elements (97). A more profound analysis of the barriers was recently carried out on the basis of Jarzynski equality. This seminal theorem links nonequilibrium work functions, as they are recorded in these forced unfolding experiments, with equilibrium energies. Their free-energy reconstruction provided folding energies that ranged from 500 k_BT for bacteriorhodopsin to more than 800 k_BT for the sodium-proton antiporter (98).

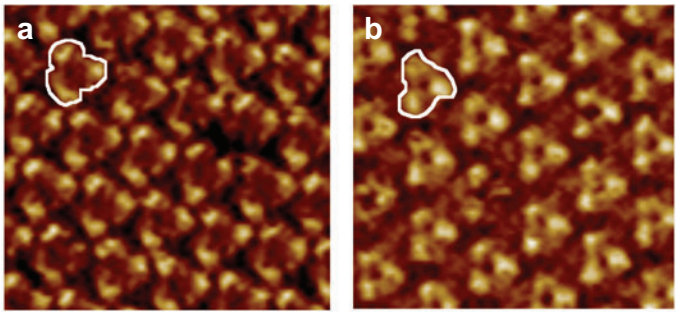

Figure 7

Unfolding of bacteriorhodopsin from the cytoplasmic and the extracellular side. (*a*) AFM image of the cytoplasmic and (*b*) of the extracellular surfaces. The distinct differences allow the unambiguous identification of the surface prior to single-molecule force spectroscopy experiments. (*c*) Unfolding traces and best-fit analysis of the different barrier positions when bacteriorhodopsin is pulled from the cytoplasmic side. (*d*) The same as in panel *c* but pulled from the extracellular side. (*e*) Schematics of the different barrier positions in the bacteriorhodopsin structure when pulled at the C terminus. (*f*) The same as in panel *e* but when the tip is pulled at the N terminus.

Unfolding from Different Ends

Membrane proteins like bacteriorhodopsin have a preferred orientation. The different sides of the membrane make different ends of the membrane protein easily accessible for single-molecule force spectroscopy. The individual structural elements of the protein may be unfolded in reversed order. This offers several advantages. When one might argue in the first instance that the unfolding barriers are approached from the back side, it becomes clear in a more profound analysis that entirely different unfolding pathways are taken when the protein is unfolded from the N- and the C-terminal ends, respectively. Nevertheless, certain barriers, e.g., hydrogen bonds or salt bridges, may be highly localized and therefore give rise to a peak in the unbinding force when approached from either side. Kessler & Gaub (95) demonstrated this for bacteriorhodopsin, which they unfolded from the cytoplasmic and the extracellular sides (see **Figure 7**). For each branch of the unfolding trace, they fitted an elasticity curve and localized the barrier. It is interesting to note that the peak heights of the unfolding forces, and thus the apparent barrier height, dropped as unfolding increased. This is interpreted as decreasing interaction with the protein's local environment because parts of the protein may be extracted already. By contrast, nonspecific interactions between the tip and sample often camouflage the first few nanometers of the unfolding trace. The two sets of traces recorded from the two sides thus contain complementary information. A summary of the barrier positions and heights found in bacteriorhodopsin when probed from both sides is sketched in **Figure 8**.

Surprisingly, barriers were located not only in or between those structural elements, which are known to be stiff, e.g., α-helical rods, but also in loops that are not well resolved in structural investigations (71–77, 95). In certain cases, the barrier positions were found to coincide with each other when probed from both sides. These barriers are of

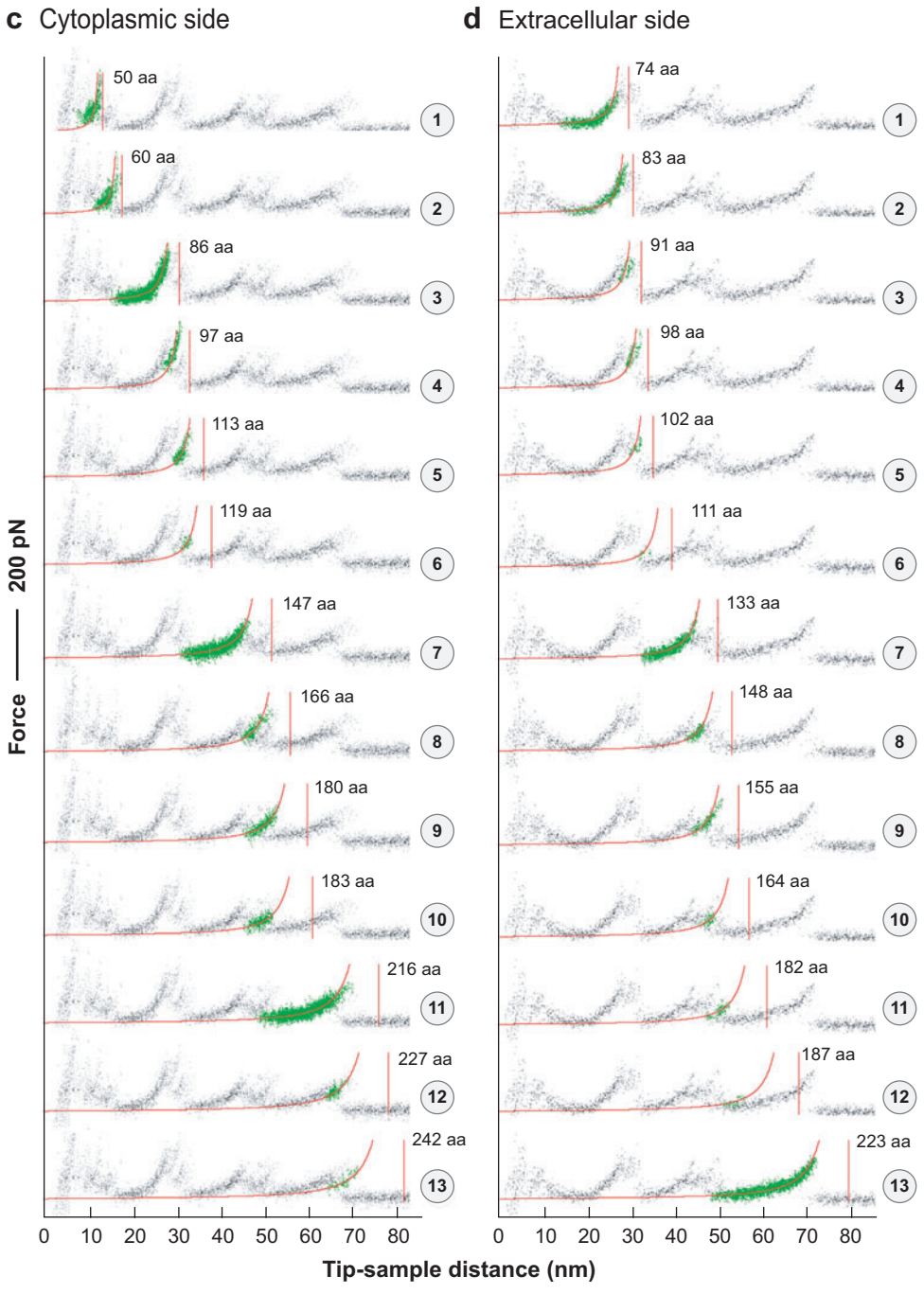

Figure 7

(*Continued*)

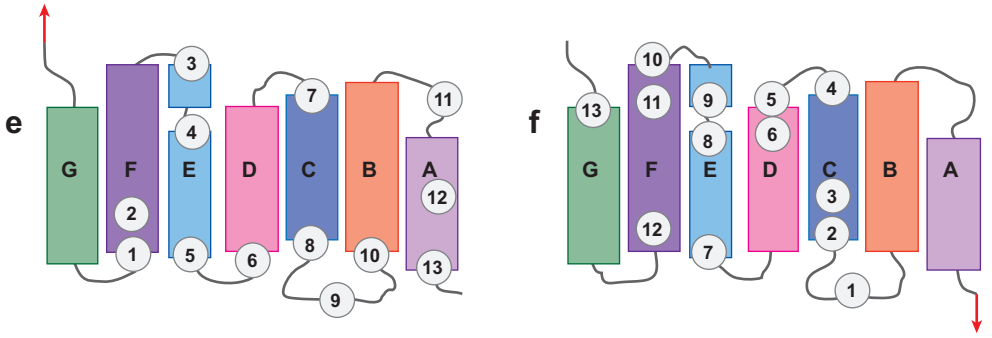

Figure 7

(*Continued*)

particular interest because they must be stabilized in both directions, upstream and downstream. In one case, the segment of the protein between this given position and the C terminal was already extracted, whereas in the other case, the segment toward the N terminal was still integrated in the membrane when the barrier was probed.

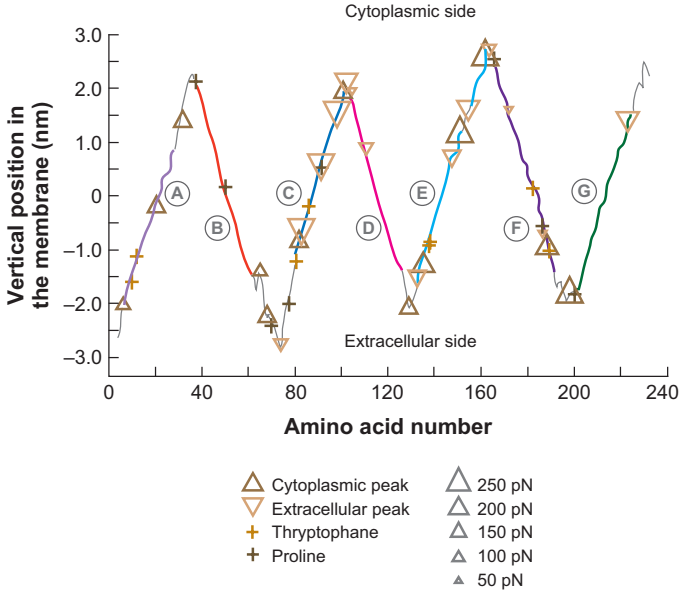

Figure 8

Schematic depiction of the barrier positions in a plot of the amino acid positions in the membrane against the sequence. The different helices are highlighted in the same colors as in **Figure 7**. The size and the orientation of the triangles encode the barrier height and the direction of unfolding.

Refolding Back into the Bilayer

With improved instrumentation and sophisticated control strategies, the handling of membrane proteins became possible at the level of individual helices. The next logical steps were then to allow the proteins to refold into the membrane and to investigate this process as a paradigm for protein folding. Kedrov et al. (99) succeeded to do so with the sodium-proton antiporter, and Kessler et al. (100) refolded individual helices of bacteriorhodopsin. **Figure 9** shows the protocol of such an experiment. First, bacteriorhodopsin was partially unfolded, and then the tip was lowered again, allowing the protein to reassemble in the membrane. As can be seen, at a certain point, the protein pulled the cantilever down. This means that mechanical work was exerted by the protein against the cantilever (see green area under the curve in **Figure 9**). Subsequent unfolding confirmed that helices E&D were fully refolded. However, Kessler et al. also reported that the majority of the folding attempts resulted in an imperfect refolding, which they attributed to both the rearrangement of the void in the membrane but also to inadequate drift stability over the prolonged time spans needed for this kind of experiment (100). Because such experiments provide both the work of unfolding and the work of refolding, they may be the foundation for a future analysis using a more fundamental nonequilibrium theorem, the Crooks theorem.

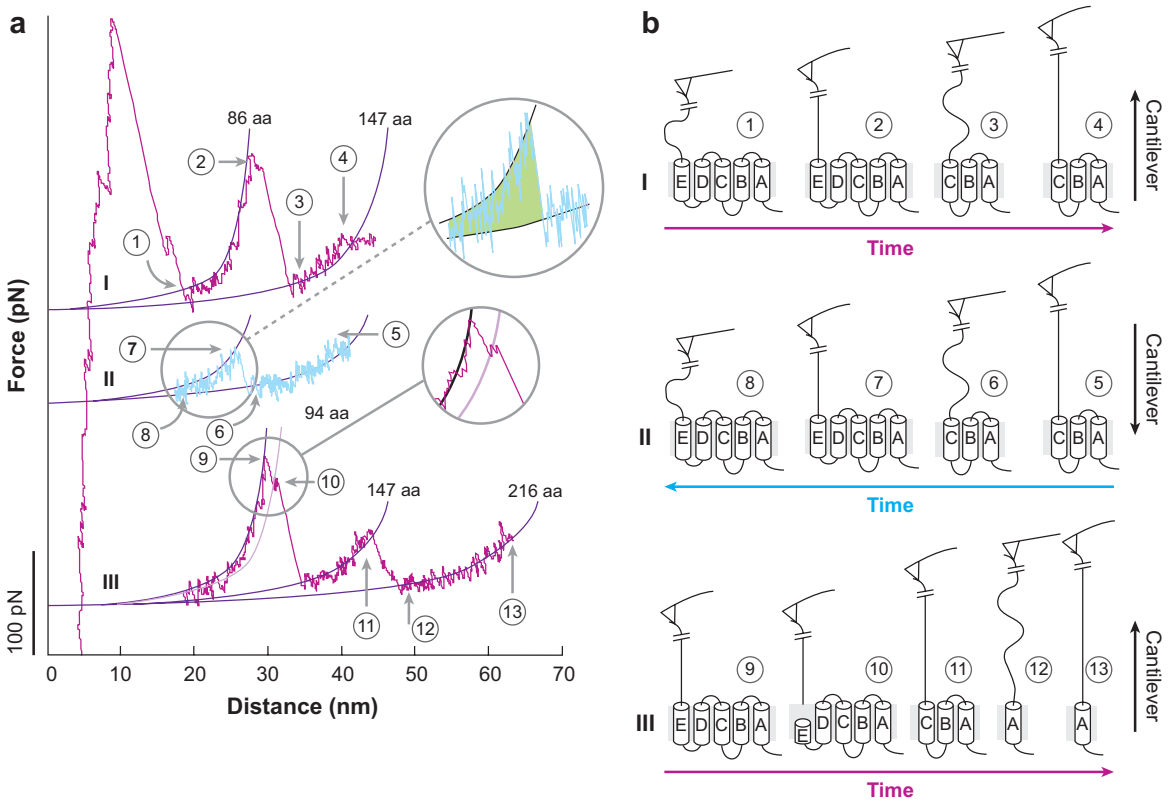

Figure 9

(*a*) Unfolding (*pink traces*) and (*b*) refolding traces of bacteriorhodopsin (*blue traces*) and schematic representation of the experiment. (*a*) Helices E and D were first extracted from the membrane. Then the cantilever was lowered again, and the force was recorded at which the membrane pulled the two helices in again. A subsequent unfolding confirms the complete refolding. The mechanical work performed by the membrane is highlighted in green (100).

Localizing Ligand Binding

The vast majority of prescribed drugs interact with membrane proteins. In view of the lack of high-resolution structural data, novel approaches to quantify and localize ligand binding to these proteins are needed. Energy barriers may not only be signatures of the intramolecular bonds, they may also be modulated by the interaction of ligands with the protein. With the option to localize such barriers with the precision of a few amino acids, an attempt to screen the potential landscape of the protein for signatures of ligand interaction seems not only feasible but moreover highly attractive.

The lab of Daniel Müller (74) demonstrated for the first time that this is possible, and the results are shown in **Figure 10**. They unfolded the sodium-proton antiporter in its active and its inactive state. As can be seen, an additional peak appears at an extension of roughly 65 nm upon activation in neutral pH. This can be attributed to a novel barrier around aa 225, which is located in the middle of helix V. A functional inhibition by 40 μM 2-aminopyrimidine, however, results in the formation of a new barrier at around aa 85, which is located in the loop between helix X and XI. The authors interpret this unexpected finding with a ligand-induced stabilization of the

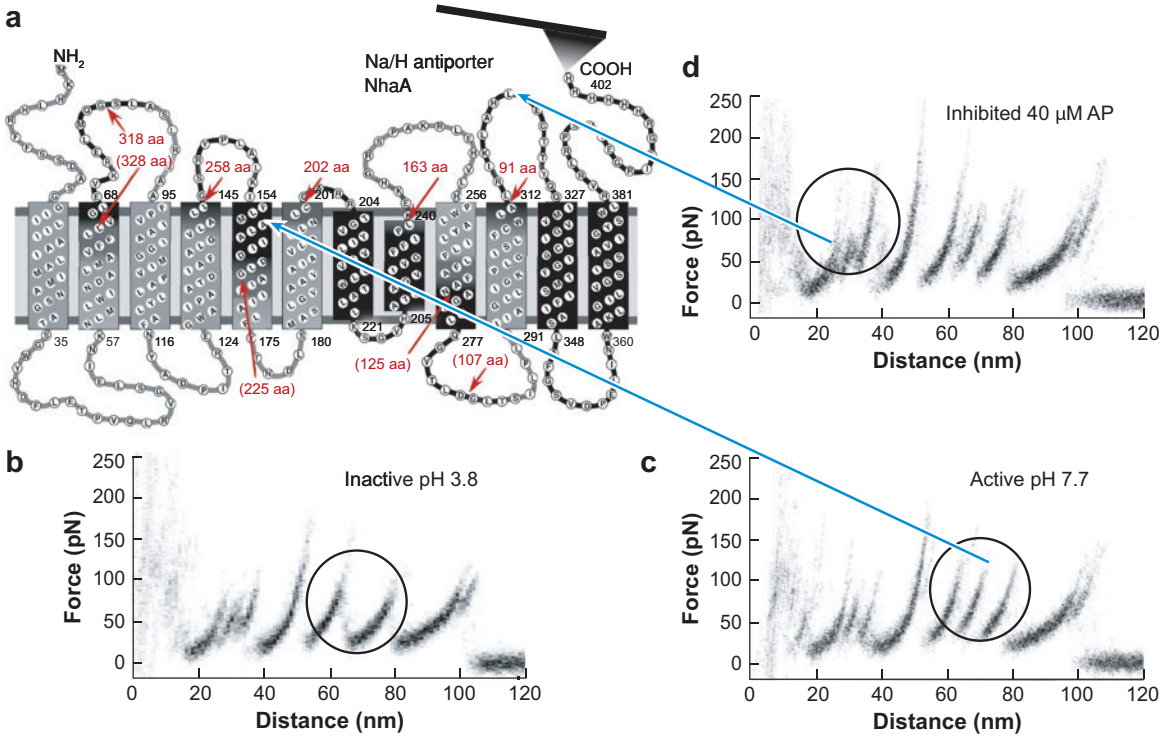

Figure 10

Modulation of unfolding barriers in sodium-proton (Na/H) antiporter by activation and ligand binding. (*a*) Schematics of the experiment. (*b*) Unfolding pattern of the inactive protein. (*c*) A new barrier appears at aa 225 upon pH-induced activation. (*d*) Ligand binding induces a new barrier in the loop around aa 85 (redrawn with permission from Reference 74).

loop, which together with other parts of the protein may form the binding pocket. This pioneering experiment opens the path for more ligands and binding pockets to be identified in the long list of health-relevant membrane proteins when no high-resolution structural information is available.

PERSPECTIVES

The AFM is currently the only instrument that allows the structure and dynamics of membrane protein surfaces to be assessed under physiological conditions at a lateral resolution of 0.5 nm and a vertical one of 0.1 nm. High-resolution imaging of surface-exposed loops allows the dynamics of membrane proteins to be monitored at subnanometer level (20). New avenues emerge for assessing not only the surface topography at high spatial resolution but also the local electronic properties of single-membrane proteins (12). Nanomanipulation of membrane protein surfaces and protein unfolding at the single-molecule level have been fully documented, and protocols for such experiments are well established (16, 101). Protein unfolding experiments can now be analyzed quantitatively and understood to the single-amino acid level (5, 74, 95, 100) and provide indirect information on the three-dimensional atomic structure of the addressed proteins and their interaction with ligands, adjacent proteins, and lipids. All these emerging data are not only complementary to structural information from crystallography and NMR

spectroscopy, but often they are the only structural data available when related proteins are not amenable to conventional high-resolution structural analyses. Recent advances in high-resolution imaging of native membranes (34, 53, 54, 102, 103) suggest exciting applications of AFM technology for the study of biological systems. This development fosters great expectations for future progress in assessing membrane proteins in their native environment by AFM, identifying specific proteins by their surface structure, and assessing their nanomechanical as well as electronic properties in situ.

DISCLOSURE STATEMENT

The authors are not aware of any biases that might be perceived as affecting the objectivity of this review.

ACKNOWLEDGMENTS

This work has been supported by the Maurice E. Müller Foundation of Switzerland, the National Center of Competence in Research on Nanoscale Science, the Swiss National Foundation grant 3100-059415 (A.E.), as well as by the Munich Center for Integrated Protein Science (H.E.G.). The authors thank Daniel Müller, Mathias Rief, Stefan Kufer, and Hermann Gumpp for the numerous insightful and constructive discussions.

LITERATURE CITED

1. Engelman DM. 2005. *Nature* 438:578–80
2. Simons K, Ikonen E. 1997. *Nature* 387:569–72
3. Engel A, Müller DJ. 2000. *Nat. Struct. Biol.* 7:715–18
4. Oesterhelt F, Oesterhelt D, Pfeiffer M, Engel A, Gaub HE, Müller DJ. 2000. *Science* 288:143–46
5. Kedrov A, Janovjak H, Sapra KT, Müller DJ. 2007. *Annu. Rev. Biophys. Biomol. Struct.* 36:233–60
6. Binnig G, Quate CF, Gerber C. 1986. *Phys. Rev. Lett.* 56:930–33
7. Frederix PLTM, Hoogenboom BW, Fotiadis D, Müller DJ, Engel A. 2004. *MRS Bull.* 29:449–55
8. Hansma PK, Cleveland JP, Radmacher M, Walters DA, Hillner PE, et al. 1994. *Appl. Phys. Lett.* 64:1738–40
9. Hoogenboom BW, Hug HJ, Pellmont Y, Martin S, Frederix PLTM, et al. 2006. *Appl. Phys. Lett.* 88:193109
10. Ando T, Kodera N, Takai E, Maruyama D, Saito K, Toda A. 2001. *Proc. Natl. Acad. Sci. USA* 98:12468–72
11. Picco L, Bozec L, Ulcinas A, Engledew D, Antognozzi M, et al. 2007. *Nanotechnology* 18:044030

11a. Schitter G, Åström KJ, DeMartini BE, Thurner PJ, Turner KL, Hansma PK. 2007. *IEEE Trans. Control Syst. Technol.* 15:906–15

12. Frederix P, Gullo M, Akiyama T, Tonin A, de Rooij N, et al. 2005. *Nanotechnology* 16:997–1005
13. Chon JWM, Mulvaney P, Sader JE. 2000. *J. Appl. Phys.* 87:3978–88
14. Yokokawa M, Wada C, Ando T, Sakai N, Yagi A, et al. 2006. *EMBO. J.* 25:4567–76
15. Müller DJ, Amrein M, Engel A. 1997. *J. Struct. Biol.* 119:172–88

16. Müller DJ, Engel A. 2007. *Nat. Protoc.* 2:2191–97
17. Müller DJ, Fotiadis D, Scheuring S, Müller SA, Engel A. 1999. *Biophys. J.* 76:1101–11
18. Müller DJ, Büldt G, Engel A. 1995. *J. Mol. Biol.* 249:239–43
19. Müller DJ, Heymann JB, Oesterhelt F, Möller C, Gaub H, et al. 2000. *Biochim. Biophys. Acta* 1460:27–38
20. Scheuring S, Müller DJ, Stahlberg H, Engel HA, Engel A. 2002. *Eur. Biophys. J.* 31:172–78
21. Cisneros DA, Oesterhelt D, Müller DJ. 2005. *Structure* 13:235–42
22. Müller DJ, Engel A. 1999. *J. Mol. Biol.* 285:1347–51
23. Schabert FA, Henn C, Engel A. 1995. *Science* 268:92–94
24. Czajkowsky D, Sheng S, Shao Z. 1998. *J. Mol. Biol.* 276:325–30
25. Fotiadis D, Hasler L, Müller DJ, Stahlberg H, Kistler J, Engel A. 2000. *J. Mol. Biol.* 300:779–89
26. Fotiadis D, Suda K, Tittmann P, Jeno P, Philippsen A, et al. 2002. *J. Mol. Biol.* 318:1381–94
27. Scheuring S, Ringler P, Borgnia M, Stahlberg H, Müller DJ, et al. 1999. *EMBO J.* 18:4981–87
28. Pogoryelov D, Yu J, Meier T, Vonck J, Dimroth P, Müller DJ. 2005. *EMBO Rep.* 6:1040–44
29. Seelert H, Poetsch A, Dencher NA, Engel A, Stahlberg H, Müller DJ. 2000. *Nature* 405:418–19
30. Stahlberg H, Müller DJ, Suda K, Fotiadis D, Engel A, et al. 2001. *EMBO Rep.* 21:1–5
31. Fotiadis D, Qian P, Philippsen A, Bullough PA, Engel A, Hunter CN. 2004. *J. Biol. Chem.* 279:2063–68
32. Scheuring S. 2006. *Curr. Opin. Chem. Biol.* 10:387–93
33. Scheuring S, Reiss-Husson F, Engel A, Rigaud JL, Ranck JL. 2001. *EMBO J.* 20:3029–35
34. Fotiadis D, Liang Y, Filipek S, Saperstein DA, Engel A, Palczewski K. 2003. *Nature* 421:127–28
35. Liang Y, Fotiadis D, Filipek S, Saperstein DA, Palczewski K, Engel A. 2003. *J. Biol. Chem.* 278:21655–62
36. Suda K, Filipek S, Palczewski K, Engel A, Fotiadis D. 2004. *Mol. Membr. Biol.* 21:435–46
37. Guo W, Shi L, Filizola M, Weinstein H, Javitch JA. 2005. *Proc. Natl. Acad. Sci. USA* 102:17495–500
38. Jastrzebska B, Fotiadis D, Jang GF, Stenkamp RE, Engel A, Palczewski K. 2006. *J. Biol. Chem.* 281:11917–22
39. Fotiadis D, Jastrzebska B, Philippsen A, Müller DJ, Palczewski K, Engel A. 2006. *Curr. Opin. Struct. Biol.* 16:252–59
40. Bouvier M. 2001. *Nat. Rev. Neurosci.* 2:274–86
41. Terrillon S, Bouvier M. 2004. *EMBO Rep.* 5:30–34
42. Bayburt TH, Leitz AJ, Xie G, Oprian DD, Sligar SG. 2007. *J. Biol. Chem.* 282:14875–81
43. James JR, Oliveira MI, Carmo AM, Iaboni A, Davis SJ. 2006. *Nat. Methods* 3:1001–6
44. Scheuring S, Seguin J, Marco S, Levy D, Robert B, Rigaud JL. 2003. *Proc. Natl. Acad. Sci. USA* 100:1690–93
45. Scheuring S, Rigaud JL, Sturgis JN. 2004. *EMBO J.* 23:4127–33
46. Bahatyrova S, Frese RN, Siebert CA, Olsen JD, Van Der Werf KO, et al. 2004. *Nature* 430:1058–62
47. Scheuring S, Busselez J, Levy D. 2005. *J. Biol. Chem.* 280:1426–31
48. Goncalves RP, Bernadac A, Sturgis JN, Scheuring S. 2005. *J. Struct. Biol.* 152:221–28
49. Scheuring S, Goncalves RP, Prima V, Sturgis JN. 2006. *J. Mol. Biol.* 358:83–96

50. Scheuring S, Buzhynskyy N, Jaroslawski S, Goncalves RP, Hite RK, Walz T. 2007. *J. Struct. Biol.* 160:385–94
51. Scheuring S, Sturgis JN. 2005. *Science* 309:484–87
52. Mannella CA. 1984. *Science* 224:165–66
53. Hoogenboom BW, Suda K, Engel A, Fotiadis D. 2007. *J. Mol. Biol.* 370:246–55
54. Goncalves RP, Buzhynskyy N, Prima V, Sturgis JN, Scheuring S. 2007. *J. Mol. Biol.* 369:413–18
55. Andersen C, Schiffler B, Charbit A, Benz R. 2002. *J. Biol. Chem.* 277:41318–25
56. Yildiz O, Vinothkumar KR, Goswami P, Kühlbrandt W. 2006. *EMBO J.* 25:3702–13
57. Akiyama T, Gullo MR, de Rooij NF, Staufer U, Tonin A, et al. 2003. *Insulated conductive cantilevers for in situ experiments in structural biology*. Presented at 12th Int. Conf. Scanning Tunn. Microsc./Spectrosc. Relat. Tech., Eindhoven
58. Gullo MR, Frederix PL, Akiyama T, Engel A, de Rooij NF, Staufer U. 2006. *Anal. Chem.* 78:5436–42
59. Gullo MR, Akiyama T, Frederix P, Tonin A, Staufer U, et al. 2005. *Microelectron. Eng.* 78–79:571–74
60. Goncalves RP, Agnus G, Sens P, Houssin C, Bartenlian B, Scheuring S. 2006. *Nat. Methods* 3:1007–12
61. Clausen-Schaumann H, Seitz M, Krautbauer R, Gaub HE. 2000. *Curr. Opin. Chem. Biol.* 4:524–30
62. Müller DJ, Baumeister W, Engel A. 1999. *Proc. Natl. Acad. Sci. USA* 96:13170–74
63. Scheuring S, Stahlberg H, Chami M, Houssin C, Rigaud JL, Engel A. 2002. *Mol. Microbiol.* 44:675–84
64. Rief M, Gautel M, Oesterhelt F, Fernandez JM, Gaub HE. 1997. *Science* 276:1109–12
65. Rief M, Oesterhelt F, Heymann B, Gaub HE. 1997. *Science* 275:1295–97
66. Seitz M, Friedsam C, Jostl W, Hugel T, Gaub HE. 2003. *ChemPhysChem* 4:986–90
67. Hugel T, Grosholz M, Clausen-Schaumann H, Pfau A, Gaub H, Seitz M. 2001. *Macromolecules* 34:1039–47
68. Blank K, Morfill J, Gaub HE. 2006. *ChemBioChem* 7:1349–51
69. Grandbois M, Beyer M, Rief M, Clausen-Schaumann H, Gaub HE. 1999. *Science* 283:1727–30
70. Müller DJ, Heymann JB, Oesterhelt F, Möller C, Gaub H, et al. 2000. *Biochim. Biophys. Acta* 1460:27–38
71. Park PS, Sapra KT, Kolinski M, Filipek S, Palczewski K, Müller DJ. 2007. *J. Biol. Chem.* 282:11377–85
72. Janovjak H, Knaus H, Müller DJ. 2007. *J. Am. Chem. Soc.* 129:246–47
73. Preiner J, Janovjak H, Rankl C, Knaus H, Cisneros DA, et al. 2007. *Biophys. J.* 93:930–37
74. Kedrov A, Krieg M, Ziegler C, Kühlbrandt W, Müller DJ. 2005. *EMBO Rep.* 6:668–74
75. Kedrov A, Wegmann S, Smits SH, Goswami P, Baumann H, Müller DJ. 2007. *J. Struct. Biol.* 159:290–301
76. Möller C, Fotiadis D, Suda K, Engel A, Kessler M, Müller DJ. 2003. *J. Struct. Biol.* 142:369–78
77. Müller DJ, Baumeister W, Engel A. 1999. *Proc. Natl. Acad. Sci. USA* 96:13170–74
78. Rief M, Gautel M, Gaub HE. 2000. *Adv. Exp. Med. Biol.* 481:129–41
79. Carrion-Vazquez M, Oberhauser AF, Fowler SB, Marszalek PE, Broedel SE, et al. 1998. *Proc. Natl. Acad. Sci. USA* 96:3694–99
80. Rief M, Pascual J, Saraste M, Gaub HE. 1999. *J. Mol. Biol.* 286:553–61
81. Friedsam C, Wehle AK, Kuhner F, Gaub HE. 2003. *J. Phys. Condens. Matter* 15:S1709–23

82. Evans E, Ludwig F. 1999. *J. Phys. Condens. Matter* 11:1–6
83. Grater F, Shen JH, Jiang HL, Gautel M, Grubmüller H. 2005. *Biophys. J.* 88:790–804
84. de Groot BL, Grubmüller H. 2001. *Science* 294:2353–57
85. Lu H, Isralewitz B, Krammer A, Vogel V, Schulten K. 1998. *Biophys. J.* 75:662–71
86. Grubmüller H, Heymann B, Tavan P. 1996. *Science* 271:997–99
87. Marszalek PE, Lu H, Li H, Carrion-Vazquez M, Oberhauser AF, et al. 1999. *Nature* 402:100–3
88. Kellermayer MS, Smith SB, Granzier HL, Bustamante C. 1997. *Science* 276:1112–16
89. Kreuzer HJ, Wang RLC, Grunze M. 1999. *New. J. Phys.* 21. doi:10.1088/1367-2630/1/1/321
90. Livadaru L, Netz RR, Kreuzer HJ. 2003. *Macromolecules* 36:3732–44
91. Li H, Rief M, Oesterhelt F, Gaub HE. 1999. *Appl. Phys. A Mater. Sci. Process.* 68:407–10
92. Li HB, Rief M, Oesterhelt F, Gaub HE, Zhang X, Shen JC. 1999. *Chem. Phys. Lett.* 305:197–201
93. Hugel T, Rief M, Seitz M, Gaub HE, Netz RR. 2005. *Phys. Rev. Lett.* 94:048301
94. Neuert G, Hugel T, Netz RR, Gaub HE. 2006. *Macromolecules* 39:789–97
95. Kessler M, Gaub HE. 2006. *Structure* 14:521–27
96. Müller DJ, Kessler M, Oesterhelt F, Möller C, Oesterhelt D, Gaub H. 2002. *Biophys. J.* 83:3578–88
97. Janovjak H, Kessler M, Oesterhelt D, Gaub H, Müller DJ. 2003. *EMBO J.* 22:5220–29
98. Preiner J, Janovjak H, Rankl C, Knaus H, Cisneros DA, et al. 2007. *Biophys. J.* 93:930–37
99. Kedrov A, Ziegler C, Janovjak H, Kühlbrandt W, Müller DJ. 2004. *J. Mol. Biol.* 340:1143–52
100. Kessler M, Gottschalk KE, Janovjak H, Müller DJ, Gaub HE. 2006. *J. Mol. Biol.* 357:644–54
101. Müller D, Engel A. 2008. *Curr. Opin. Colloid Interface Sci.* In press
102. Buzhynskyy N, Sens P, Prima V, Sturgis JN, Scheuring S. 2007. *Biophys. J.* 93:2870–76
103. Buzhynskyy N, Hite RK, Walz T, Scheuring S. 2007. *EMBO Rep.* 8:51–55
104. Scheuring S, Boudier T, Sturgis JN. 2007. *J. Struct. Biol.* 159:268–76
105. Urry DW, Hugel T, Seitz M, Gaub HE, Sheiba L, et al. 2002. *Philos. Trans. R. Soc. Lond. Ser. B.* 357:169–84

Annual Review of Biochemistry

Volume 77, 2008

Contents

Prefatory Chapters

Single-Molecule Theme

Recent Advances in Biochemistry

Indexes

Errata

An online log of corrections to *Annual Review of Biochemistry* articles may be found at http://biochem.annualreviews.org/errata.shtml